Electrical resistivity and thermoelectric power of a quasi-one-dimensional Nb_3Te_4 single crystal inserted with mercury: $Hg_xNb_3Te_4$

1999 J. Phys.: Condens. Matter 11 6373

(http://iopscience.iop.org/0953-8984/11/33/307)

J. Phys.: Condens. Matter **11** (1999) 6373–6384. Printed in the UK PII: S0953-8984(99)02932-X

Electrical resistivity and thermoelectric power of a quasi-one-dimensional Nb_3Te_4 single crystal inserted with mercury: $Hg_xNb_3Te_4$

Takanori Kagohashi, Tukasa Takarada, Hitoshi Hasegawa, Yuriko Katumata, Masanori Kuga, Hiroyuki Okamoto, Hiroshi Kaneko and Yutaka Ishihara

Department of Physics, Faculty of Science, Kanazawa University, Kanazawa 920-1192, Japan

Received 23 May 1999, in final form 8 June 1999

Abstract. The electrical resistivity and the thermoelectric power of Nb_3Te_4 inserted with mercury have been measured in the temperature range from 1.4 to 300 K. The magnitude of the resistivity and the residual-resistivity ratio are not greatly affected by addition of Hg. The magnitude of the resistive anomaly at 90 K increases when adding a small amount of Hg but begins to decrease at about $x = 0.03$ and is no longer visible at about $x = 0.15$. Similarly, the magnitude of the resistive anomaly at 30 K decreases with increasing Hg concentration and disappears at about $x = 0.26$. The thermoelectric power S also shows two anomalies at about 90 and 30 K. The anomaly of S at 90 K becomes smeared by addition of Hg and disappears at about $x = 0.3$. The anomaly of S at 30 K becomes clear by addition of Hg and is still present at an amount of $x = 0.8$. The sign of S is negative at all measured temperatures for $x < 0.3$ and is positive at temperatures below 7 K for $x > 0.3$. The superconducting transition temperature is enhanced from 1.9 to 5.4 K by addition of Hg. The upper critical fields parallel ($H_{c2\parallel}$) and perpendicular ($H_{c2\perp}$) to the c axis have been measured near T_C. The critical fields show large anisotropy for $x \geqslant 0.3$: the ratio $H_{c2\parallel}/H_{c2\perp}$ is about 5 for $x < 0.3$ and 40 for $x \geqslant 0.3$. These results are discussed on the basis of the multiband model with electron-like and hole-like carriers and with phonon drag.

1. Introduction

The intercalation effects on the electrical properties for layered compounds have been studied intensively. In these compounds, intercalation often induces drastic changes in the physical properties of host crystals such as superconductivity. Such effects are principally caused by a remarkable increase in the lattice constants and by charge transfer between intercalated atom and mother crystal. The combination of Nb with other atoms into Nb_3X_4, with X = S, Se, Te, has negligible influence on the lattice constants as compared with layered compounds [1–3]. Hence, the insertion effect for Nb_3X_4 will mainly be caused by a charge transfer between the inserted atom and the mother crystal. Then, the compounds are suitable for the study of the effect of insertion on the electrical properties of host crystals without changing their lattice constants or energy-band structure.

The crystal structure of Nb_3X_4 is a hexagonal crystal system [4–6]. Figure 1(a) shows a projected view of Nb_3Te_4 along the c axis. The unit cell contains six niobium atoms and eight chalcogens as shown in figure 1(a). Each niobium atom is surrounded by six chalcogens at the corner of a deformed octahedron of NbX_6. The solid lines in figure 1(a) emphasize these octahedra. The octahedron forms a three-dimensional network: each octahedron is linked to two other octahedra by common faces and to four octahedra by common edges. The niobium

0953-8984/99/336373+12$30.00

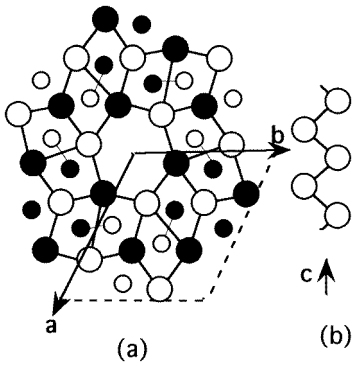

Figure 1. Crystal structure of Nb_3Te_4 (a) viewed along the *c* axis. Nb atoms are indicated by small circles and chalcogen atoms by large circles. Atoms on the plane with $z = c/4$ are drawn by solid circles and atoms on the plane with $z = 3c/4$ by open circles. The structure is built up by $NbTe_6$ octahedra that are shown by solid lines. Fine lines show Nb–Nb chains. Dot lines show the unit cell. (b) Zigzag Nb chain along the *c* axis.

atoms are shifted from the centres of the octahedra in the direction of faces sharing two edges with other octahedra. Hence, zigzag Nb–Nb chains are formed along the *c* axis as shown in figure 1(b). The Nb–Nb distance in the chains ($d_\parallel = 2.973$ Å) is comparable to the corresponding value in niobium metal (2.859 Å). The shortest Nb–Nb distances between Nb chains are $d_\perp = 3.854$ Å. The ratio of $d_\perp$ to $d_\parallel$ is 1.296. Thus, this large anisotropy leads to weak coupling between Nb chains. Another remarkable feature of Nb_3X_4 structure is the presence of large infinite empty channels along the *c* axis as shown by the hexagon in figure 1(a).

Reflecting the quasi-one-dimensional crystal structure, Nb_3X_4 shows large anisotropy in the electrical properties such as resistivity in the normal state [7], upper critical field [8–10] and magnetization in the superconducting state [11]. Furthermore, in both Nb_3S_4 [7] and Nb_3Se_4 [9] the electrical resistivity shows the T^3 temperature dependence below 80 K, which can be explained in terms of carrier–carrier Umklapp scattering in the quasi-one-dimensional energy band structure [12]. The electrical resistivity and the thermoelectric power of Nb_3Te_4 show two anomalies at about 90 and 30 K [13]. The anomaly at 90 K is caused by a charge-density-wave formation (CDW formation) with commensurate wave vectors [14, 15]. For the anomaly at 30 K, superlattice-diffraction spots have not been observed yet. However, we believe that the anomaly is also caused by another CDW formation. This is because the magnitude of the resistive anomaly changes with lithium insertion [16]. The thermodynamic properties in the superconducting state of Nb_3X_4 have been studied in detail by Okamoto and Ishihara *et al* [11, 17]. These properties also show large anisotropies and follow the weak-coupling BCS theory including effects of an energy-gap anisotropy [18].

Oshiyama has made a calculation of the energy-band structure of Nb_3X_4 using the linear-combination-of-atomic-orbitals method [12, 19]. Owing to the presence of three niobium chains in the unit cell, three conduction bands exist and correspondingly three Fermi surfaces. The calculated Fermi surfaces reflect the quasi-one-dimensional crystal structure: these Fermi surfaces consist of warped planelike sheets [19]. The bandwidths along the chain directions are highly dispersive and are in the range of 1.5–2.5 eV, while those along the interchain directions are quite flat and are of the order of 0.1 eV. The ratios of the conduction-band width along the chain direction to that along the perpendicular direction are 15, 18 and 19 for X = S, Se and Te. For the band structure of Nb_3S_4, Bullet [20] and Canadell and Whangbo [21] have also obtained similar results by an atomic-orbital method and a tight-binding approximation

on the basis of the extended Hückel method. Further, Canadell and Whangbo indicated that the Fermi surfaces of Nb_3X_4 could be significantly modified by alkali-metal intercalation.

Many inserted compounds $A_xNb_3X_4$ with A = metal atom were prepared using various methods [1–3, 16, 22]. Electrical properties of $A_xNb_3X_4$ have been measured by Ishihara *et al* [16] and by Ohtani *et al* [3]. However, detailed electrical properties of a single crystal of $A_xNb_3X_4$ have not been studied yet. The present measurements are the first in detail on single crystals.

In this paper we report the electrical properties and the thermoelectric power of Nb_3Te_4 single crystals inserted with mercury by means of exposing Nb_3Te_4 to mercury vapour. The upper critical fields have also been measured to study the effect of mercury insertion on the superconducting property of Nb_3Te_4.

2. Experimental procedure

A single crystal of binary compound Nb_3Te_4 was prepared by an iodine-vapour-transport method following Nakada and Ishihara [23, 24] on the basis of the earlier work [6, 25]. The powder forms of Nb and Te were mixed in stoichiometric ratio. The mixture was put in a quartz ampoule of inner diameter 12–13 mm and length 15 cm together with 70–90 mg of iodine. The ampoule was put in the furnace with a temperature difference of 40 K between the two ends of the ampoule. The mixture was put at the low temperature end (1.23×10^3 K) of the ampoule. The crystals grew between both ends of the ampoule. The purity of the elements is 99.6% for niobium and 99.999% for tellurium. The grown crystals were examined by x-ray diffraction analysis using a four-circle goniometer and were identified to be Nb_3Te_4. The grown crystals were always fibres and were elongated parallel to the *c* axis. For mercury insertion, the ternary element and single crystals of Nb_3Te_4 in the desired molar ratio were sealed in an evacuated quart tube under about 1 Pa. Then, the tube was kept at 7.0×10^2 K for 7 days. The purity of mercury was 99.99%. If there was no residual mercury, the nominal value was used as Hg concentration for a given crystal.

The lattice constants of $Hg_xNb_3Te_4$ were determined with a powder x-ray diffractometer using Cu Kα radiation. The electrical resistivity was measured along the *c* axis using a dc four-contact method in the temperature range from 1.4 to 300 K. The upper critical fields were measured by monitoring the resistance while sweeping a magnetic field at constant temperature. The thermoelectric power was measured using a conventional dc two-probe method in the temperature range from near T_C to 250 K. The samples were clamped between two sapphire plates with a constant temperature difference of about 0.3–0.5 K, maintained by means of an electric heater. The contacts were silver paint. The samples used for the electrical and thermoelectric measurements were typically about 12 mm long and 0.12–0.16 mm in diameter.

3. Results

Figure 2 shows the lattice constants of $Hg_xNb_3Te_4$ at room temperature for a concentration range of $x \leqslant 0.77$. The values of lattice constants *a* and *c* slightly increase linearly with increasing Hg concentration. These values at $x = 0.77$ are about 0.2% larger than those of pure Nb_3Te_4. Then, the volume of the unit cell for $x = 0.77$ increases by about 0.6% with respect to pure Nb_3Te_4: both lattice constants are not greatly affected in spite of the large amount of Hg inserted. The values of both lattice constants for pure Nb_3Te_4 are in good agreement with those of Selte and Kjekshus [4].

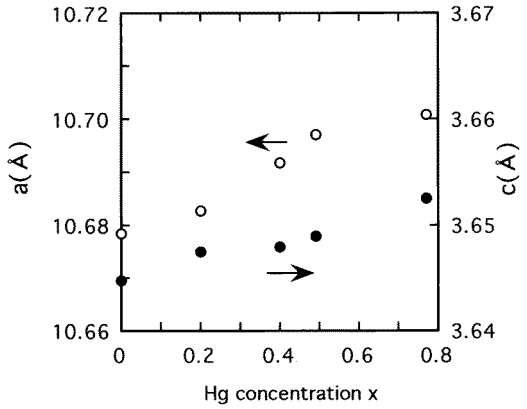

Figure 2. Hg concentration dependence of the lattice constants a and c of $Hg_xNb_3Te_4$ at room temperature.

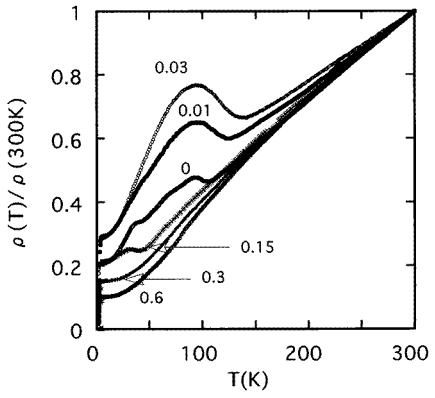

Figure 3. Temperature dependence of the resistivity of $Hg_xNb_3Te_4$ for typical Hg concentrations. Data are normalized to each other at 300 K. The number for each curve in the figure shows the x value.

Figure 3 shows the typical resistivities, normalized to the room-temperature value along the c axis, as a function of temperature for various Hg concentrations. In figure 3, pure Nb_3Te_4 clearly shows two resistive anomalies at about 90 K (here referred to as the upper anomaly) and at about 30 K (here referred to as the lower anomaly). The magnitude of the upper anomaly increases at low concentrations below $x = 0.03$. For x values above 0.03, in contrast, the magnitude of the anomaly decreases with increasing Hg concentration and is no longer visible at about $x = 0.15$. The onset temperature at which the anomaly occurs is enhanced from 105 to 135 K for $x = 0.03$. However, the peak temperature, at which the resistivity indicates the maximum value in the resistive anomaly, is independent of Hg concentration and is 92 ± 3 K, while the peak temperature of the lower anomaly is not clear except at concentrations of around $x = 0.15$. The onset temperature does not change with addition of Hg and is about 42 K. The magnitude of the lower anomaly decreases with increasing Hg concentration in the same manner as the upper anomaly and disappears at about $x = 0.26$. The resistivity of pure Nb_3Te_4, which grew near the low temperature end

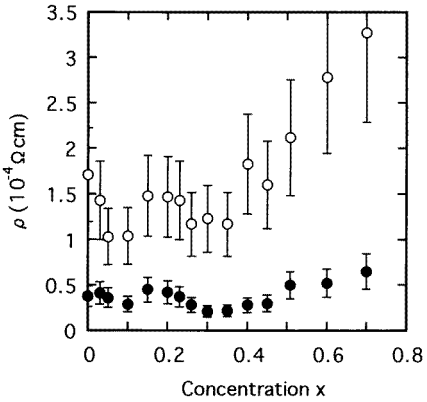

Figure 4. Hg concentration dependence of the resistivity of $Hg_xNb_3Te_4$ at 6 and 300 K. Solid and open circles are the resistivities at 6 and 300 K.

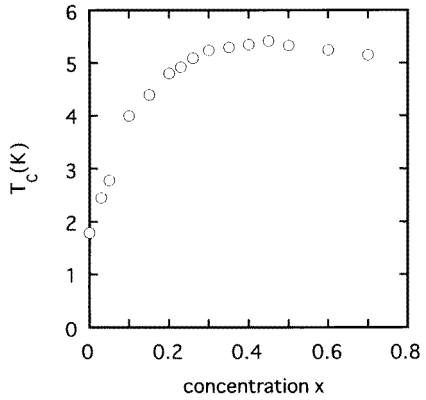

Figure 5. Hg concentration dependence of the superconducting transition temperature T_C of $Hg_xNb_3Te_4$.

of the crystal-growth ampoule, showed a large hysteresis loop near 100 K [15]. However, the resistivity of pure Nb_3Te_4 that grew near the high temperature end showed a very small and broad hysteresis loop near 100 K. For $Hg_xNb_3Te_4$, no hysteresis was observed at either transition.

Figure 4 shows the resistivity along the *c* axis of $Hg_xNb_3Te_4$ at 6 K in the residual resistivity temperature range and at 300 K for various Hg concentrations. The data are somewhat scattered. The error was about 30%, mainly due to the inaccuracy in size measurements because of the small size of the sample and the sample dependence of the resistivity in host crystal: the resistivity of Nb_3Te_4 is somewhat different from sample to sample, and seems to depend on the sample quality. The magnitude of the resistivity for $x < 0.3$ does not change by Hg insertion within the experimental error, while for concentrations of $x \geqslant 0.3$ the magnitude of the resistivity is slightly increasing with increasing Hg concentration. The residual resistivity ratio $\rho(300\ \mathrm{K})/\rho(6\ \mathrm{K})$ is about 4–6 for $x < 0.3$ and 5–8 for $x \geqslant 0.3$.

Figure 5 shows the dependence of the superconducting transition temperature T_C on the Hg concentration. With addition of Hg, T_C increases steeply from 1.9 to 5.4 K and turns

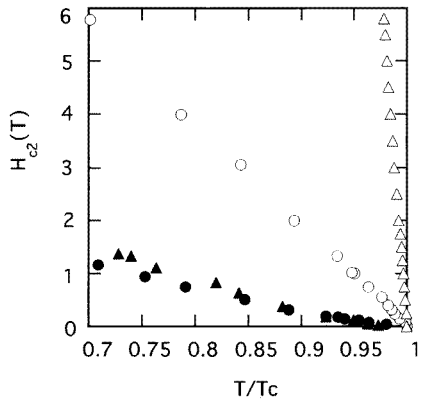

Figure 6. Upper-critical-field curves of $Hg_xNb_3Te_4$ for x values of 0.1 and 0.7 plotted on a reduced temperature scale (T/T_C). Open circles ($H_{c2\parallel}$) and solid circles ($H_{c2\perp}$) are the upper critical fields parallel and perpendicular to the c axis for $x = 0.1$. Open triangles ($H_{c2\parallel}$) and solid triangles ($H_{c2\perp}$) are the upper critical fields parallel and perpendicular to the c axis for $x = 0.7$.

to decrease slightly at $x = 0.4$. The width of the transition temperature is about 0.3 K and is independent of Hg concentration. This fact indicates that the inserted Hg atoms are distributed uniformly in the sample. The transition temperature is defined as the temperature where the resistivity becomes one-half of that in the normal state. The transition width is taken as the temperature difference between the points where the transition was 10% and 90% complete.

Figure 6 shows the temperature dependence of the upper critical fields H_{c2} for x values of 0.1 and 0.7. In the figure, $H_{c2\parallel}$ and $H_{c2\perp}$ are upper critical fields parallel and perpendicular to the c axis. The remarkable feature of the critical fields is that $H_{c2\perp}$ is almost independent of x value. The critical field $H_{c2\perp}$ exhibits a slight positive curvature close to T_C as has been found in layered superconductors. The temperature dependence of $H_{c2\perp}$ in the reduced temperature T/T_C range from 0.95 to 0.7 is linear, while the critical field $H_{c2\parallel}$ is proportional to temperature in the reduced temperature range of 1–0.7.

At this point it is worthwhile to examine the dimensionality of the system. Despite its needlelike morphology and linear-chain-crystal structure, Nb_3Te_4 is probably not one dimensional in the sense of KCP and TTF–TCNQ. This is because the absence of a Peierls transition to an insulating state implies that the entire Fermi surface is not affected by the CDW gap. However, the increase in the resistivity suggests that a fraction of the Fermi surface is affected, i.e., the nesting criterion is satisfied by a fraction of the Fermi surface. Thus, the upper critical field could be treated by the anisotropic Ginzburg–Landau theory, which relates H_{c2} to the coherence lengths [26, 27] by

$$H_{c2} = \Phi_0/2\pi\xi_a\xi_b \tag{1}$$

where Φ_0 is the flux quantum and ξ_a and ξ_b are two principal coherence lengths in the plane perpendicular to the applied magnetic field. Since the upper critical fields are almost proportional to $\Delta T = T_C - T$ in the temperature range measured, we assume that the typical formula of the temperature dependence of $\xi(T) = \xi(0)/(1 - T/T_C)^{1/2}$ holds for Nb_3Te_4 inserted with mercury. The coherence lengths $\xi(0)$ at 0 K are, therefore, related to the slopes

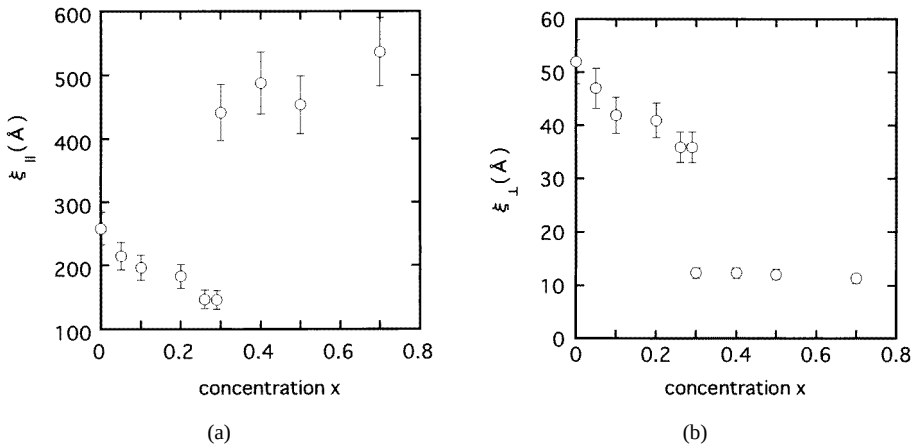

(a) (b)

Figure 7. Hg concentration dependence of the coherence length: (a) coherence length $\xi_{\parallel}(0)$ parallel to the c axis and (b) coherence length $\xi_{\perp}(0)$ perpendicular to the c axis.

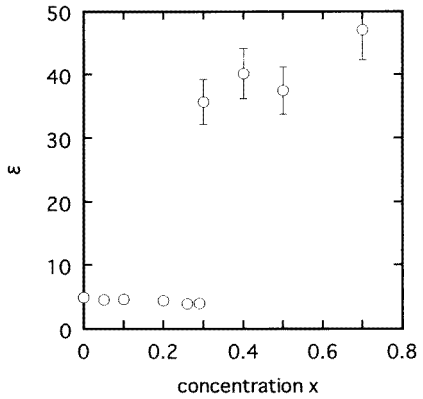

Figure 8. Hg concentration dependence of the anisotropy $\varepsilon = \xi_{\parallel}(0)/\xi_{\perp}(0)$ of coherence lengths.

of H_{c2} versus T using equation (1) as follows:

$$\frac{\mathrm{d}H_{c2\parallel}}{\mathrm{d}T} = -\frac{\Phi_0}{2\pi\xi_{\perp}^2(0)T_C} \tag{2}$$

$$\frac{\mathrm{d}H_{c2\perp}}{\mathrm{d}T} = -\frac{\Phi_0}{2\pi\xi_{\parallel}(0)\xi_{\perp}(0)T_C} \tag{3}$$

where $\xi_{\parallel}(0)$ and $\xi_{\perp}(0)$ are the coherence lengths parallel and perpendicular to the c axis.

Figures 7(a) and 7(b) show the Hg concentration dependence of the coherence lengths $\xi_{\parallel}(0)$ and $\xi_{\perp}(0)$ obtained by using equations (2) and (3). Both $\xi_{\parallel}(0)$ and $\xi_{\perp}(0)$ decrease monotonically from 259 ± 26 and 52 ± 3 to 146 ± 15 and 36 ± 2 Å with increasing Hg concentration up to near $x = 0.3$. At an x value of 0.3, $\xi_{\parallel}(0)$ increases abruptly from 146 to 450 ± 45 Å and, in contrast, $\xi_{\perp}(0)$ decreases from 36 to 12 ± 1 Å. For x values above 0.3, both $\xi_{\parallel}(0)$ and $\xi_{\perp}(0)$ are almost independent of Hg concentration. Figure 8 shows the ratio $\varepsilon = \xi_{\parallel}(0)/\xi_{\perp}(0)$ for various Hg concentrations. The ratio is about 5 for $x < 0.3$ and 40 for $x \geqslant 0.3$. The data of $\xi_{\parallel}(0)$ are somewhat scattered. The error for $\xi_{\parallel}(0)$ was about 10%,

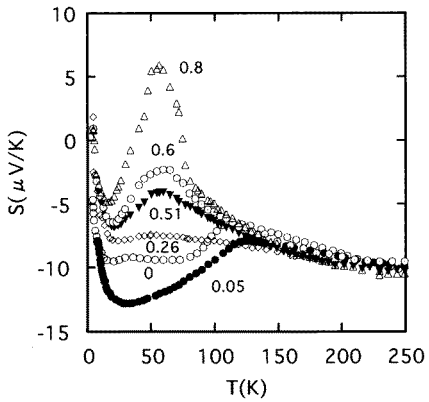

Figure 9. Temperature dependence of the thermoelectric power S of $Hg_xNb_3Te_4$. The number for each curve in the figure is the x value.

mainly due to the positive curvature in $H_{c2\perp}$ near T_C. That is, the estimate of the coherence length involves the upper critical field slope $dH_{c2\perp}/dT$ at T_C, which cannot be determined in a straightforward way, because of the positive curvature in $H_{c2\perp}$ near T_C. To avoid this ambiguous procedure we take the slope in the range of linear temperature dependence of $H_{c2\perp}$.

Figure 9 shows the absolute thermoelectric power S for pure Nb_3Te_4 and Nb_3Te_4 inserted with mercury. The data were corrected for the thermoelectric power of lead using the table of Roberts [28]. The data for pure Nb_3Te_4 were taken from [16]. The behaviour of the thermoelectric power can be divided into two temperature ranges: at temperatures above and below 130 K. Above this temperature, the magnitude of the thermoelectric power hardly changes with Hg addition, with a negative slope. The sign of the thermoelectric power is negative over this temperature range. On the other hand, at temperatures below 130 K, the magnitude of S greatly changes with Hg addition. The two CDW transitions are easily observable as sharp changes in slope at about 110 and 35 K. The increase in the thermoelectric power at 110 and 35 K coincides with the temperature of the anomaly in the resistivity. The broad minimum value at 90 K smears with increasing Hg concentration and is no longer visible at about $x = 0.3$. Such behaviour is in good agreement with that of the resistivity. In contrast, the shallow minimum value at 25 K becomes deeper with addition of Hg and is still present even at $x = 0.8$. At temperatures between 130 and 30 K, the thermoelectric power decreases at first but turns to increase with increasing Hg concentration and shows a maximum value at about 60 K. The maximum value becomes more definite and increases with increasing Hg concentration. For the sample with $x = 0.8$, the sign of the thermoelectric power is positive at temperatures between 30 and 80 K. At low temperatures below about 20 K, the thermoelectric power decreases towards zero for x values below 0.3, having a negative sign. However, the sign of the thermoelectric power for x values above 0.3 changes from negative to positive at about 7 K.

4. Discussion

As mentioned above, the three conduction bands in Nb_3Te_4 give rise to three Fermi surfaces [17]: the outermost Fermi surface, the intermediate Fermi surface and the innermost Fermi

surface. The outer two Fermi surfaces consist of warped planelike sheets. The innermost Fermi surface also has some planelike regions, although there are small hole-pockets around the M-point of the Brillouin zone. The interaction between the niobium chains introduces warping of the Fermi surfaces. From the structure of the Fermi surfaces one could expect the formation of a CDW corresponding to the lower anomaly as well as the upper anomaly. Then, although superlattice-diffraction spots corresponding to the lower anomaly have not been observed yet, we believe that the anomaly is also caused by another CDW formation. Owing to the contribution from two Fermi surfaces among the three, we can understand the effect of Hg insertion on the resistive anomalies at 90 and 30 K as follows: insertion of Hg will modify the shape of the Fermi surfaces of Nb_3Te_4 by transfer of 6s electrons of the Hg atom into the conduction bands. An additional contribution can be expected from the stiffening of the lattice: the insertion of atoms in the empty channels increases the three-dimensional character of the band structure by the enhancement of coupling between niobium chains, which will reduce the areas of the Fermi surface participating in the nesting. In the case, as a result of these modifications, where the area of nesting parts of Fermi surface decreases with addition of Hg, the CDW formation is suppressed. The reduction of the upper anomaly for x values above 0.03 and the lower anomaly in $Hg_xNb_3Te_4$ is expected to correspond to this case. In contrast, in the case where the area of nesting parts of the Fermi surface increases with addition of impurity, the CDW formation is enhanced. The enhancement of the upper anomaly for x values below 0.03 is considered to correspond to this case.

Despite insertion of large amounts, the magnitude of the resistivity and the residual resistivity ratio of $Hg_xNb_3Te_4$ is not greatly affected. The result can be interpreted as follows: the conducting property of the host material Nb_3Te_4 is metallic and its conduction band consists of electron-like and hole-like carriers, as we shall see later. Consequently, the number of the conducting charge carriers in the host material would be much greater than that of inserted carriers from mercury. That is, the fractional change in the number of charge carriers cannot be very great with insertion of Hg. This is supported by the fact that the magnitude of the thermoelectric power does not change appreciably with insertion of Hg at temperatures above 130 K. Further, the result of the thermoelectric power indicates that although the dominant carriers are electrons at temperatures above 130 K, the number of electrons decreases and that of holes increases with increasing Hg concentration, resulting in the increase of the contribution of holes to the conductivity. The mobility of holes would slightly be smaller than that of electrons. Thus, the resistivity slightly increases as a result of reduction of the contribution of electrons to the conductivity. The fact that the residual resistivity is insensitive to insertion of Hg indicates that the electric current is caused by the conduction carriers localized on Nb chains, which mainly flows on the Nb chains, and the inserted Hg atoms do not act as impurity scatters. Namely, Hg atoms are inserted into the empty channels along the c axis. This picture for Hg distribution in the compound is supported by the fact that the lattice constants of pure Nb_3Te_4 are not greatly increased with addition of Hg.

The change in sign of the thermoelectric power for heavily inserted Nb_3Te_4 at low temperatures implies that the conduction bands of pure Nb_3Te_4 consist of electron-like and hole-like carriers, with the dominant carrier species changing from electron-like to hole-like with increasing Hg concentration. The negative increase of the thermoelectric power at 90 K in the pure sample is also interpreted in terms of the multiband model as follows: the upper CDW involves the formation of a gap on the part of the Fermi surface with hole-like carriers. The negative carriers remaining are less compensated and the thermoelectric power becomes more negative. Similarly, the CDW at 30 K produces a gap on the hole-like region remaining or on another hole-like region and the thermoelectric power becomes more negative.

With addition of mercury, there are mainly two possible causes for the smearing of the negative peak of the thermoelectric power at 90 K: (i) the fraction of the Fermi surface affected by the CDW formation decreases as in the case of the resistivity; (ii) the hole contribution to the thermoelectric power increases with increasing Hg concentration. In fact, for the sample with $x = 0.8$, the sign change of the thermoelectric power at 80 K indicates that the dominant carriers change from electrons to holes. However, the appearance of the negative peak at 25 K cannot be explained only by the CDW formation and multiband model. This is because although the magnitude of the resistive anomaly disappears at concentration of $x = 0.26$, the negative peak is observed irrespective of the magnitude of Hg concentration measured. Hence, we believe that this minimum value is associated with a phonon-drag contribution to the thermoelectric power, which is negative. Then, the thermoelectric power of pure and lightly inserted Nb_3Te_4 at low temperatures can be described as the sum of the three terms: a diffusion contribution, a phonon-drag contribution and a CDW contribution due to the formation of a gap on another part of the Fermi surface with hole-like carriers.

In order to consider the increase of T_C, although the superconductivity of $Hg_xNb_3Te_4$ is highly anisotropic, as will be seen later, the isotropic BCS theory is used here for simplicity. Then, T_C is given as follows: $T_C = 0.85\Theta \exp(-1/VN)$, where Θ, V and N are the Debye temperature, the electron–phonon coupling constant and the density of states at the Fermi level. In accordance with the equation, the increase of T_C can be explained as follows: (i) the increase of the magnitude of Θ_D by the lattice stiffening for the same reason as described above; (ii) the increase of N by restoration of the areas of the Fermi surface lost by the formation of gaps due to the CDW formation, or by the electronic-band-structure changes. However, at present, we cannot explain the effect of insertion on T_C quantitatively. This is because these parameters have not been observed yet. We are doing a further study using a calorimetric method to interpret this result quantitatively.

To examine the experimental results obtained for the superconducting states, we determined the zero-temperature coherence lengths parallel and perpendicular to the c axis, using our data for H_{c2} and equations (2) and (3). The conspicuous difference in the superconducting property between the compounds of $Hg_xNb_3Te_4$ with $x < 0.3$ and $x \geqslant 0.3$ is due to the difference of the type of transport carrier: the superconducting states for samples with $x < 0.3$ exist on the Fermi surface with electron-like carriers, whereas the superconducting states for samples with $x \geqslant 0.3$ exist on the Fermi surface with hole-like carriers. We also estimate the Ginzburg–Landau mass ratio from the relation that

$$\varepsilon^2 = [\xi_{\parallel}(0)/\xi_{\perp}(0)]^2 = m_{\perp}/m_{\parallel} \tag{4}$$

where $m_{\perp}$ and $m_{\parallel}$ are effective masses perpendicular and parallel to the c axis. The mass ratio is about 25 for $x < 0.3$ and 1.6×10^2 for $x \geqslant 0.3$. The band-structure calculation shows that the ratio of the conduction-band width along the c axis to that along the perpendicular direction is 19 for Nb_3Te_4 [12], which corresponds to a rough measure for the effective mass ratio of 25. Though it is rather difficult to make a detailed comparison between them, it may be said that the two results are not inconsistent in the conducting states with electron-like carriers. As mentioned above, according to the band-structure calculation, there are small hole-like orbits around the M point in the Brillouin zone. However, they are less anisotropic as compared with the electron-like orbits with the conduction-band-width ratio of 19. It is, therefore, difficult to understand how the large anisotropy in the hole conduction band arises from only a consideration of an anisotropic effective mass.

The crystal structure of Nb_3Te_4 consists of Nb chains running along the c axis, as described in section 1. The distance between Nb atoms in a chain is metallic, but the interchain distance exceeds the metallic distance. Hence, Nb_3Te_4 is regarded as an aggregate of one-dimensional

chains. However, the properties of such a superconductor can be considered as bulk so long as the coherence length of the crystal is larger than the interchain distance. In the case of $Hg_xNb_3Te_4$, the smallest coherence length is about 12 Å in the samples with $x \geqslant 0.3$ and is about three times larger than the interchain distance. Consequently, this estimate implies that the compound is a highly anisotropic and three-dimensional superconductor.

In summary, we have measured the resistivity, the upper critical field and the thermoelectric power of Nb_3Te_4 inserted with mercury. The sign of the thermoelectric power for x values below 0.3 is negative over the entire temperature range measured, whereas the sign of the thermoelectric power for x values above 0.3 changes from negative to positive at about 7 K. The result indicates that the transport properties of $Hg_xNb_3Te_4$ are due to multiband conduction, with the dominant carriers species changing from electron-like to hole-like with increasing Hg concentration. The anomaly of the thermoelectric power at 90 K is enhanced with light insertion but is suppressed with further insertion and disappears at $x = 0.3$. In contrast, the anomaly of the thermoelectric power at 30 K is observed irrespective of Hg concentration. Such behaviour can be explained in terms of phonon drag, which gives rise to an additional term in the thermoelectric power. With addition of Hg, the magnitude of both resistive anomalies at 90 and 30 K is suppressed and disappears by a concentration of $x = 0.26$. The magnitude of the resistivity and the residual-resistivity ratio are not greatly affected with addition of Hg, while the superconducting transition temperature is enhanced from 1.9 to 5.4 K with addition of Hg. The upper critical field parallel to the c axis changes abruptly at $x = 0.3$. Anisotropy of the upper critical fields gives an estimate for the coherence lengths parallel and perpendicular to the c axis: the value of $\xi_{\parallel}(0)$ decreases from 259 ± 26 to 146 ± 15 Å with increasing Hg concentration for $x < 0.3$ and increases abruptly to 450 ± 45 Å at $x = 0.3$. Similarly, the value of $\xi_{\perp}(0)$ decreases from 52 ± 3 to 36 ± 2 Å with increasing Hg concentration for $x < 0.3$ and decreases to 12 ± 1 Å at $x = 0.3$. The coherence-length ratio $\xi_{\parallel}(0)/\xi_{\perp}(0)$ is about 5 for $x < 0.3$ and 40 for $x \geqslant 0.3$. The effective mass ratio $m_{\perp}/m_{\parallel}$ obtained on the basis of the ellipsoidal fluxoid model is about 25 for $x < 0.3$ and 1.6×10^2 for $x \geqslant 0.3$. The superconducting states exist on the Fermi surface with electron-like carriers for $x < 0.3$ and on the Fermi surface with hole-like carriers for $x \geqslant 0.3$. There is coherence over many chains in the perpendicular direction to the c axis. For this reason, in its critical field properties $Hg_xNb_3Te_4$ is a highly anisotropic and three-dimensional superconductor.

Acknowledgment

This work was partially supported by a Grant-in-Aid for Scientific Research from the Ministry of Education, Science, Sports and Culture of Japan.

References

[1] Huan G and Greenblatt M 1987 *Mater. Res. Bull.* **22** 505
[2] Huan G and Greenblatt M 1987 *Mater. Res. Bull.* **22** 943
[3] Ohtani T, Sano Y and Yokota Y 1993 *J. Solid State Chem.* **103** 504
[4] Selte K and Kjekshus A 1964 *Acta Crystallogr.* **17** 1568
[5] Smeggil J G 1971 *J. Solid State Chem.* **3** 248
[6] Ruysink A F J, Kadijk F, Wagner A J and Jellinek F 1968 *Acta Crystallogr.* B **24** 1614
[7] Ishihara Y and Nakada I 1982 *Solid State Commun.* **42** 579
[8] Biberacher W and Schwenk H 1980 *Solid State Commun.* **33** 385
[9] Ishihara Y and Nakada I 1982 *Solid State Commun.* **44** 1439
[10] Ishihara Y and Nakada I 1983 *Solid State Commun.* **45** 129
[11] Okamoto H and Ishihara Y 1993 *Phys. Rev.* B **48** 3927

[12] Oshiyama A 1983 *J. Phys. Soc. Japan* **52** 587
[13] Ishihara Y, Nakada I, Suzuki K and Ichihara M 1984 *Solid State Commun.* **50** 657
[14] Suzuki K, Ichihara M, Nakada I and Ishihara Y 1984 *Solid State Commun.* **52** 743
[15] Sekine T, Kiuchi Y, Matsuura E and Uchinokura K 1987 *Phys. Rev.* B **36** 3153
[16] Sakai K, Ishihara Y, Okamoto H, Tsutsumi K and Lu H-Z 1991 *Solid State Commun.* **77** 73
[17] Okamoto H, Taniguti H and Ishihara Y 1996 *Phys. Rev.* B **53** 384
[18] Clem J R 1966 *Ann. Phys., NY* **40** 268
[19] Oshiyama A 1982 *Solid State Commun.* **43** 607
[20] Bullet D W 1980 *J. Solid State Chem.* **33** 13
[21] Canadell E and Whango M-H 1986 *Inorg. Chem.* **25** 1488
[22] Schöllhorn R and Schramm W 1979 *Z. Naturf.* B **34** 697
[23] Nakada I and Ishihara Y 1984 *Japan. J. Appl. Phys.* **23** 677
[24] Nakada I and Ishihara Y 1985 *Japan. J. Appl. Phys.* **24** 31
[25] Amberger E, Polborn K, Grimm P, Dietrich M and Obst B 1978 *Solid State Commun.* **26** 943
[26] De Gennes P G 1966 *Superconductivity of Metals and Alloys* (New York: Benjamin) p 100
[27] Morris R C and Coleman R V 1972 *Phys. Rev.* B **5** 895
[28] Roberts R B 1977 *Phil. Mag.* **36** 91